Transient Response of a Liquid Metal Heat Pipe

D. E. Tilton* and L. C. Chow†
University of Kentucky, Lexington, Kentucky
and
E. T. Mahefkey‡
Aero Propulsion Laboratory, Wright-Patterson Air Force Base, Ohio

The purpose of this research was to investigate the transient response of a liquid metal heat pipe under external radiant thermal loading at the condenser section. An experiment was conducted using an Inconel screen wick sodium heat pipe. The external wall axial temperature profile vs time was recorded for various radiant heat fluxes and condenser coverages. A simple one-dimensional model was developed. The theoretically determined temperature vs time profiles compared closely to those obtained experimentally. The analytical model predicts transient vapor mass flow rates and condensation/evaporation rates along the pipe for a variety of condenser heat load conditions. From this information, heat-pipe reversal and incipient failure can be predicted. The model also includes a dryout prediction based on the maximum capillary transport limit. This model can be easily modified for use with a variety of different heat-pipe designs and heat loading conditions.

Nomenclature

A_c = surface area of the condenser
A_s = surface area of the condenser radiant heat input
C = effective thermal capacity
h = enthalpy of fluid
L = length
m = mass
$\dot{m}$ = mass flow rate
$\dot{m}_{e,c}$ = evaporation or condensation rate
n = number of nodes
P_{in} = equivalent power input at the evaporator
Q_{ext} = net external heat input rate into a given section
Q_{rad} = heat rejection due to radiation
q_c = condenser external radiant heat flux
T = temperature
T_{av} = averaged temperature of radiant heater surface
t = time
X = heat-pipe axial position
ϵ = heat-pipe surface emissivity
λ = latent heat of vaporization
μ = dynamic viscosity
ρ = density
σ = Stefan-Boltzmann constant
σ_l = liquid sodium surface tension

Subscripts

c = condensation or condenser
e = evaporation or evaporator
eff = effective
l = liquid sodium
v = vapor sodium

Received April 10, 1986; presented as Paper 86-1271 at the AIAA/ASME 4th Thermophysics and Heat Transfer Conference, Boston, MA, June 2–4, 1986; revision received July 28, 1986.

*Research Assistant, Mechanical Engineering. Student Member AIAA.
†Associate Professor, Mechanical Engineering. Member AIAA.
‡Technical Area Manager, Power Technology Branch. Member AIAA.

Introduction

THE development of future high-power spacecraft requires a more fundamental understanding of transient heat-transfer mechanisms in heat pipes. The research reported here focuses on the transient response of a sodium heat pipe subjected to external thermal loading at the heat-pipe condenser. Experiments were designed and conducted using a sliding cylindrical shell radiant heater to supply the condenser heat input. The recorded data measurements included the external wall temperature distribution along the heat pipe as a function of time. An analytical model was developed to provide a prediction for the rate of increase in bulk temperature of the heat pipe resulting from a given heat input, and to provide insight into the internal transient behavior. The analytical model was solved numerically, and the experimental data was then utilized to confirm the theoretical bulk temperature rise predictions. The model was also used to make pertinent conclusions concerning the heat-pipe internal transient behavior, including heat-pipe flow reversal and incipient failure due to dryout. Failure due to exceeding the maximum operating temperature could also be predicted for a variety of heat loading conditions.

Experimental Description and Results

The experimental portion of this research involved supplying a thermal load to the condenser section of an Inconel 617 sodium heat pipe, which was initially operating in a normal steady-state condition. The screen wick design description is given in detail in Ref. 1. The important dimensions and some of the calculated wick properties are summarized in Table 1 for convenience. Performance limits testing of the heat pipe had previously been accomplished to establish the overall steady-state heat-transport capabilities of the design.[1]

The experimental apparatus design is presented in Fig. 1. The heater at the evaporator is a wound electrical resistance heater surrounded by a 0.038-m (1.5-in.)-thick ceramic fiber insulation blanket and nickel foil radiation shields. The power was supplied using a rheostat with a voltmeter and an ammeter to determine the power input. These meters gave an accuracy of ± 5.0 W. A data logger was used to scan eight radiation shielded thermocouples placed along the heat pipe and heater surface every 10 s. A complete reading of all thermocouples took 1.0 s, so all measurements were essentially simultaneous.

Table 1 Heat-pipe dimensions and wick properties

Total length L, m (in.)	0.457 (18)
Condenser length L_c, m (in.)	0.305 (12)
Evaporator length L_e, m (in.)	0.152 (6)
Outer diameter, m (in.)	0.0127 (0.5)
Inner diameter, m	0.0103
Vapor core area A_v, $\times 10^{-5}$ m^2	7.216
Vapor core radius r_v, $\times 10^{-3}$ m	5.131
Shell and wick mass, g	208.0
Sodium mass, g	8.0
Wick type	Inconel 617 screen
Screen size	100 × 100 mesh
Wick permeability K, $\times 10^{-10}$ m^2	4.2
Wick capillary radius r_c, $\times 10^{-4}$ m	1.0
Wick cross-sectional area A_w, $\times 10^{-5}$ m^2	3.71

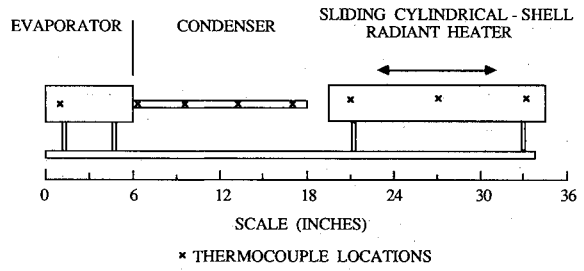

Fig. 1 Experimental setup.

For all of the experimental runs, the heat pipe was run at a steady-state temperature near 700°C. The power input at the evaporator was constant for all runs. The radiant heater was brought to an average temperature near 1000°C, and then slid concentrically onto the condenser end of the heat pipe. The surface of the sliding shell heater showed a temperature gradient of approximately 770°C at the open end to 1090°C at the closed end, according to the three thermocouples placed on the inner shell heater surface. The heater was left on until the temperature of the heat pipe neared 1000°C, which was considered the maximum temperature allowable due to the thermomechanical stress limitation based on deflection of a cantilever beam.

Table 2 shows the experimental external wall temperature profile as a function of time. Table 3 shows the corresponding shell heater surface temperature profile. The positions of the thermocouples (T_1–T_8) are indicated in Fig. 1. The thermocouple numbering begins from the left of the figure. In Table 2, T is the average of the thermocouple readings T_1–T_5. The heat pipe is operating at steady state when the condenser heat input is initiated at $t = 0$. In Table 3, T_{ave} is determined by taking the fourth root of T^4 integrated over the coverage area. This value was then used to determine the average condenser heat flux q_c using the radiation network method for two long concentric cylinders. The average heat-pipe temperature T, and the average integrated shell heater temperature T_{ave}, from Tables 2 and 3, were used for simplicity. The net heat input to the coverage area Q is

$$Q = A_s q_c - \sigma \epsilon A_s T^4 \qquad (1)$$

where $q_c = \sigma \epsilon T_{ave}^4$. Figure 2 is a representative plot of the data obtained for the 100% condenser coverage case.

Experimental Data Analysis

To compare the analytical model to the experiments conducted, an experimental data analysis was necessary. The emissivity, effective thermal capacity of the heat pipe, and convective and conductive heat losses had to be determined.

Table 2 Experimental external wall temperature profile

Coverage, %	t, s	T_1, °C	T_2, °C	T_3, °C	T_4, °C	T_5, °C	T, °C
25	0	733	705	708	712	711	713
	104	768	740	744	749	779	756
	221	779	751	754	760	784	766
	299	783	755	758	764	794	770
50	0	735	707	710	715	711	716
	78	832	805	809	843	863	830
	130	857	830	833	867	885	854
	195	871	844	847	881	898	868
75	0	729	705	708	712	708	712
	39	814	794	828	844	861	828
	65	884	860	895	910	923	894
	91	921	895	931	945	956	930
100	0	719	697	701	705	698	704
	13	780	785	811	818	827	804
	39	889	894	916	923	930	910
	65	968	969	989	996	1000	984

Table 3 Shell heater temperature, condenser heat input

Coverage, %	T_6, °C	T_7, °C	T_8, °C	T_{ave}, °C	q_c W/cm^2
25	769	959	988	769	4.7
50	820	1003	1060	890	7.2
75	827	923	1086	928	8.2
100	826	1017	1069	943	8.6

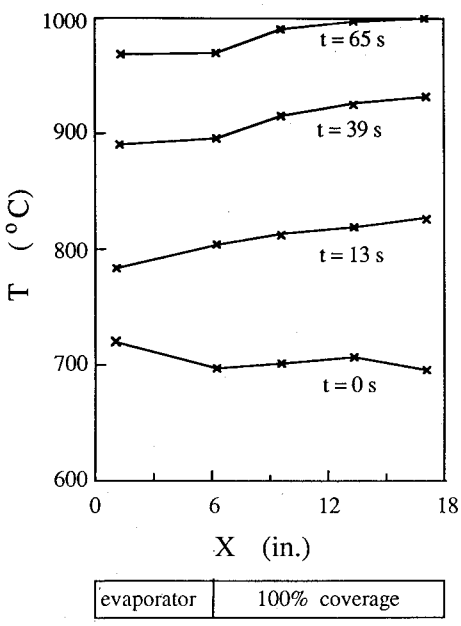

Fig. 2 External wall temperature profile transient response.

Emissivity Determination

An estimate of the emissivity was obtained by performing steady-state tests in a vacuum chamber. This was done to eliminate convective and conductive losses. The power input was equated to the heat rejected by radiation. The evaporator heat losses were neglected. The emissivity calculated in this manner was 0.7. This value was assumed to remain constant with temperature. This assumption is consistent with the experimental measurements of Olstad et al.[2]

Effective Thermal Capacity Determination

The effective thermal capacity is defined as the amount of energy needed to raise the temperature of the heat pipe by 1.0°C. The effective thermal capacity is equal to the sum of the thermal capacities of the heat-pipe shell, heat-pipe wick, sodium liquid, sodium vapor, and the heat absorbed by the liquid/vapor phase change over the unit temperature increase. The effective thermal capacity is thus defined as

$$C = C_{\text{shell}} + C_{\text{wick}} + C_l + C_v + (\Delta m/\Delta T)\lambda \qquad (2)$$

The effective thermal capacity was determined as a function of temperature using curve fits for the specific heat of Inconel 617[3] and the sodium fluid properties.[4,5] In examining the component terms, it was seen that the thermal capacities of the shell and wick are the dominant terms. Since the cross section of the heat pipe is constant along its entire length, the heat pipe can be divided into equal sections, each having the same effective thermal capacity. This is an important consideration in the analytical model described later.

Convective and Conductive Heat Losses

Since the experiment was conducted in an air environment, convection and conduction heat transfer, in addition to the dominant radiation heat transfer occurred. Rather than accounting for convection and conduction losses, an equivalent power input was used. The equivalent power input is the actual power input minus the convective and conductive losses. This is equal to the heat rejected by radiation at the steady-state operating temperature.

$$P_{\text{in}} = \sigma \epsilon A_c T^4 \qquad (3)$$

where T is the average of the external wall temperature at the initial steady-state condition. Since the convective losses are small in comparison to the radiative losses, the increase in convective losses with increasing temperature can be neglected. This method was chosen primarily because there was insufficient experimental data available to determine precise convective and conductive losses.

Analytical Model Description

A simple, one-dimensional analytical model was developed to predict the transient response of the heat pipe and to aid in understanding the experimentally observed phenomena. The model was developed to correspond to the experimental conditions in which a heat pipe operating at steady state is subjected to condenser heat input. No publications that treat this problem were found in the literature. The model is based on the principles of conservation of energy and mass. This model can be used to predict the bulk heat-pipe temperature response resulting from a variety of heat loading conditions. The local wall temperatures are not predicted. The vapor mass flow rates and the evaporation/condensation rates are predicted as a function of axial heat-pipe position.

Model Assumptions

The analytical model is based on two assumptions. The heat pipe is assumed to be completely isothermal at any given time. This assumption neglects the slight variation in vapor core temperature and the resistances to heat transfer in the shell and wick. The variation in vapor core temperature was predicted by Tien and Rohani[6] by numerically solving the Navier-Stokes equations for a similar heat pipe in the same range of operation. They showed the variation to be on the order of 1°C. Neglecting the resistances in the wall and wick results in a uniform wall temperature. The data in Table 2 indicates that this is a fairly good assumption. The second assumption is that the effective thermal capacity is uniform, as discussed earlier. These assumptions allow the overall energy storage rate to be related to a sectional energy storage rate, as will be shown in the following subsection.

Conservation of Energy

Conservation of energy is first applied to obtain a prediction for the rate of heat-pipe bulk temperature rise. This is done by equating the total net heat input to the heat rejected and the energy stored.

$$P_{\text{in}} = Q_{\text{rad}} - A_s q_c + C\frac{dT}{dt} \qquad (4)$$

If the heat pipe is assumed to be completely isothermal at every given instant in time, the bulk energy storage rate can be related to a sectional energy storage rate. If the heat pipe is divided into n equal sections, the sectional energy storage rate becomes $\bar{C}(dT/dt)$, where $\bar{C} = C/n$. Now, conservation of energy can be applied to each individual section to determine condensation/evaporation rates. Writing an energy balance for any given section yields (see Fig. 3)

$$[Q_{\text{ext}}]_i + [(\dot{m}_v h_v)_{\text{in}} + (\dot{m}_l h_l)_{\text{in}}]_i = [(\dot{m}_v h_v)_{\text{out}} + (\dot{m}_l h_l)_{\text{out}}]_i + \left[\bar{C}\frac{dT}{dt}\right]_i \qquad (5)$$

where $[Q_{\text{ext}}]_i$ is the net external heat input rate into the ith section. The liquid enthalpy flow terms in Eq. (5) can be neglected since $h_v \gg h_l$. It will be shown in the following subsection that the vapor storage is also negligible. Therefore,

$$(\dot{m}_{v,\text{out}} - \dot{m}_{v,\text{in}})_i \approx (\dot{m}_{e,c})_i \qquad (6)$$

where $(\dot{m}_{e,c})_i$ is the evaporation (+) or condensation (−) rate of the ith section. Since $h_v \approx \lambda$, Eq. (5) can be rewritten as

$$(Q_{\text{ext}})_i - (\dot{m}_{e,c}\lambda)_i = \left[\bar{C}\frac{dT}{dt}\right]_i \qquad (7)$$

Therefore, writing the sectional energy balances gives a set of equations that relate evaporation/condensation rate to the net external heat input into that section of the pipe, and the previously determined sectional energy storage rate. Equation (7) can be used to calculate the evaporation/condensation rates for all nodes at all time increments. Equation (7) indicates that if the net external heat input to any given section is less than $\bar{C}(dT/dt)$, the additional heat needed to raise the temperature of that section at the required rate must be delivered by condensing vapor in that section. Conversely, if it is greater, the excess heat must be removed by evaporating liquid.

Conservation of Mass, Vapor Phase

The next step in the model development involves using the principle of conservation of mass to determine the mass flow rates along the length of the heat pipe. Since the evaporation and condensation rates have already been determined by the equations in the previous section, writing the equation for conservation of mass for the vapor at each section gives the mass flow rates (see Fig. 4).

$$(\dot{m}_{\text{in}})_i + (\dot{m}_{e,c})_i = (\dot{m}_{\text{out}})_i + \left(\frac{dm}{dt}\right)_i \qquad (8)$$

The term dm/dt can be calculated using the known dT/dt and the density of sodium vapor as a function of temperature. It was found that dm/dt was several orders of magnitude smaller than the other terms in Eq. (8) [$\dot{m} \sim \mathcal{O}(0.1)$ g/s and $dm/dt \sim \mathcal{O}(10^{-5})$ g/s], and could therefore be neglected.

Now, Eq. (8) can be written for all nodes at all time steps to determine the mass flow rates since $(\dot{m}_{e,c})_i$ and the end conditions are known.

Analytical Model Solution Procedure

Starting from a steady-state condition, a condenser heat input is initiated. The overall energy balance [Eq. (4)] is

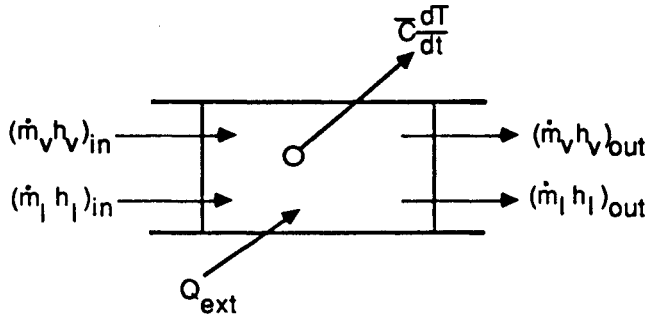

Fig. 3 Sectional energy balance.

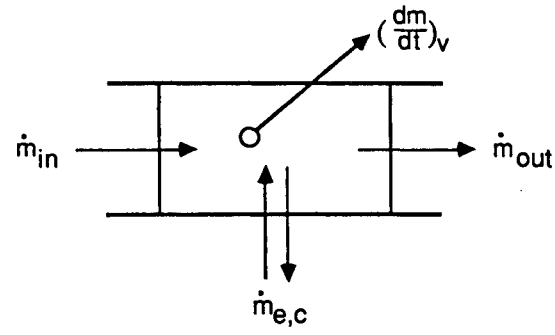

Fig. 4 Sectional vapor mass balance.

applied to determine the heat-pipe bulk energy storage rate $[C(dT/dt)]$. This is divided by the number of equal sections to determine the sectional energy storage rate $[\bar{C}(dT/dt)]$. Equation (7) is then applied to all sections to determine local evaporation/condensation rates. Next, conservation of mass is applied to determine local mass flow rates [Eq. (8)]. Last, the time step is incremented, and the procedure is repeated until the desired time has elapsed.

Experimental and Theoretical Results

In this section, the experimental and analytical model results are compared. The comparisons include various imposed heat fluxes and condenser coverages. The model predictions for local evaporation/condensation and mass flow rates are also presented and discussed.

Temperature Profile Comparison

The theoretical prediction for rate of bulk temperature rise compared closely to the experimental results for all of the cases. The maximum deviation between the average heat-pipe temperature and the model prediction was less than 10°C at any given time step. Figure 5 shows this comparison for the 8.6-W/cm^2 condenser radiant heat flux and 100% condenser coverage. The temperature values used for the experimental plot come from the average value given in Table 2. Figure 6 shows the experimental and analytical results comparison for the 25% condenser coverage and 4.7-W/cm^2 condenser radiant heat flux case.

Evaporation and Condensation Rate Prediction

Figures 7 and 8 indicate the locations of the evaporation and condensation zones along the length of the heat pipe. For example, Figure 7 shows the evaporation and condensation zones at various times for the 8.6-W/cm^2 case. The evaporation and condensation rates at 30 s are seen to be significantly lower than the evaporation and condensation rates at the initial steady state. Since the net external heat input at the evaporator is constant, the difference between the heat going into evaporation and that applied externally must go into storage. Similarly, at the condenser, the heat applied to the wall both by vapor condensation and by the external shell heater all goes into storage. At 60 s, the total net external heat input into the heat pipe has decreased due to the rising temperature of the heat pipe. Therefore, less heat goes into storage, and the evaporation and condensation rates increase.

Figure 8 can be analyzed in a similar fashion. For this 4.7-W/cm^2 case, the total net external heat input is much less than the 8.6-W/cm^2 case due to the reduction in heat flux as well as the coverage area. Consequently, the evaporation and condensation rates do not change significantly anywhere except in the condenser heat input zone. The condenser heat input simply increases the temperature of the heat pipe to the point where the additional heat input can be rejected by an increase in the heat radiated from the uncovered portion of the condenser.

In general, according to Eq. (7), whenever the net external heat input into a given section is less than $\bar{C}(dT/dt)$, condensation will occur. Whenever it is greater, evaporation occurs.

Mass Flow Rate Prediction

Examples of the theoretical vapor mass flow predictions can be seen in Figs. 9 and 10 for the 8.6-W/cm^2 and the 4.7-W/cm^2 cases, respectively. The curves given at 0 s reflect the initial steady-state condition. For both cases, the condenser radiant heat input remained on until after 60 s had elapsed. Negative values indicate vapor mass flow in the opposite direction.

The mass flow rate of the vapor transports heat from sections of higher net heat input to sections of lower net heat input. Therefore, the greater the difference in net heat input between any two sections is, the greater the vapor mass flow rate will be. Figure 9 shows that the vapor mass flow rates in the heat pipe are much lower at 30 s than at the initial steady state. This is because the difference between the net heat input into the evaporator and the net heat input into the condenser is less at 30 s. At 60 s, the net heat input into the condenser is reduced due to the rising temperature of the heat pipe. Consequently, the difference between the net heat input at the evaporator and that at the condenser becomes greater and the vapor mass flow rates increase. If the condenser net heat input were greater than the evaporator net heat input, the vapor flow would reverse.

Figure 10 can be analyzed in a similar fashion. In this case, the heat pipe actually operates like two smaller heat pipes. The point on each curve where the mass flow rate equals zero can be considered as a fictitious dividing boundary between the two smaller heat pipes. The region of condenser heat input becomes an evaporator for the second heat pipe. The 30-s and 60-s curves show the time-dependent location of the dividing boundary. As can be seen, the vapor flows in opposite directions on either side of the boundary.

Dryout Prediction

A prediction for wick dryout was incorporated into the model. This prediction results from the capillary wicking limit equation.[7]

$$Q_{\max} = \dot{m}_{\max}\lambda = \left[\frac{\rho_l K A_w \lambda}{\mu_l L_{\text{eff}}}\right]\left[\frac{2\sigma_l}{r_c}\right] \tag{9}$$

The maximum heat-transport rate $Q_{\max}$, calculated according to Eq. (9) for various temperatures, is summarized in Table 4. It should be noted that the value used for L_{eff} in the calculation of maximum heat flux is independent of the radiant heat flux condenser coverage. According to Eq. (7), a condenser radiant heat input large enough to reach the maximum heat flux value will cause condensation to occur in the evaporator. Even though less condensation would occur in the original

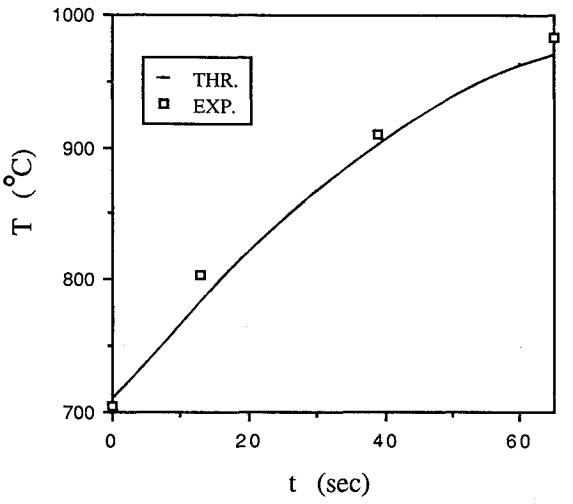

Fig. 5 Rate of bulk temperature increase comparison, 8.6 W/cm², 100% coverage.

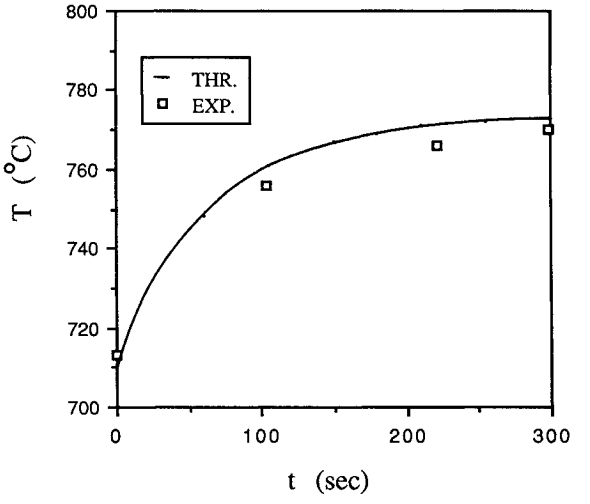

Fig. 6 Rate of bulk temperature increase comparison, 4.7 W/cm², 25% coverage.

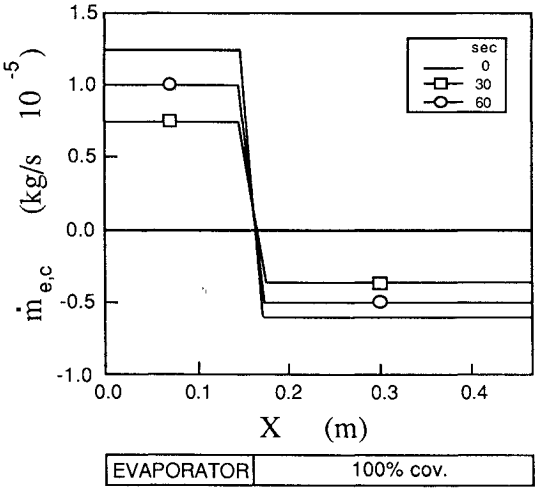

Fig. 7 Theoretical evaporation/condensation rate prediction, 8.6 W/cm², 100% coverage.

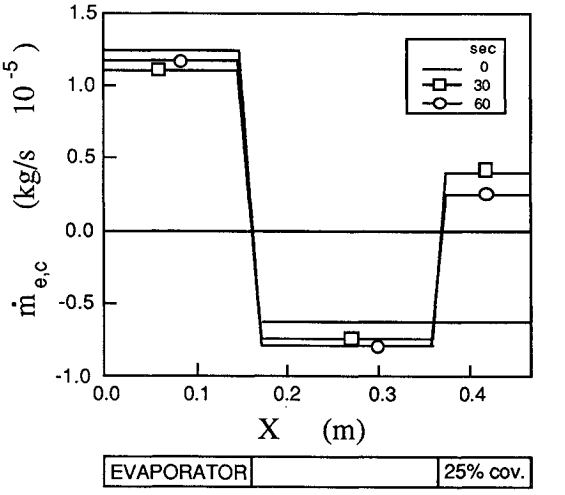

Fig. 8 Theoretical evaporation/condensation rate prediction, 4.7 W/cm², 25% coverage.

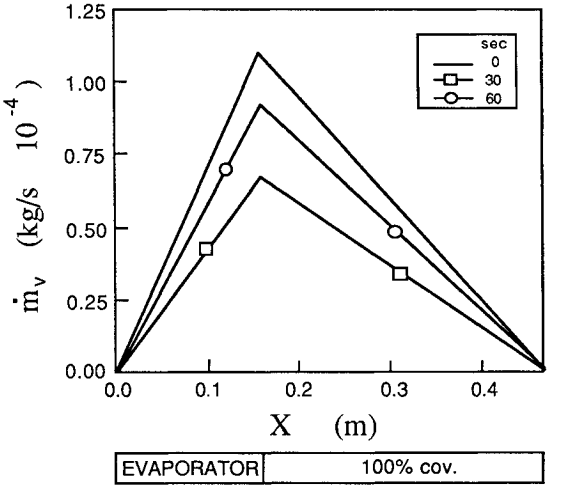

Fig. 9 Theoretical vapor mass flow rate prediction, 8.6 W/cm², 100% coverage.

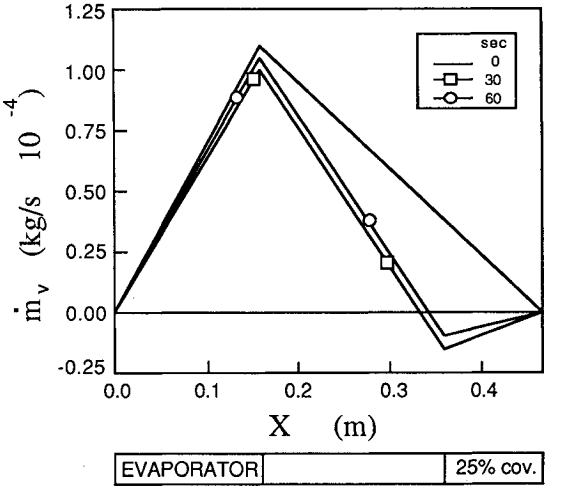

Fig. 10 Theoretical vapor mass flow rate prediction, 4.7 W/cm², 25% coverage.

Table 4 Maximum heat-transport rate

Temperature, K	Q_{max}, W
900	3047
1000	3024
1100	2781
1173	2619
1273	2438
1350	2044

Table 5 Dryout prediction

Coverage, %	q_c, W/cm^2	$A_s q_c$, W
25	123.8	3764
50	80.1	4870
75	73.7	6721
100	85.7	10421

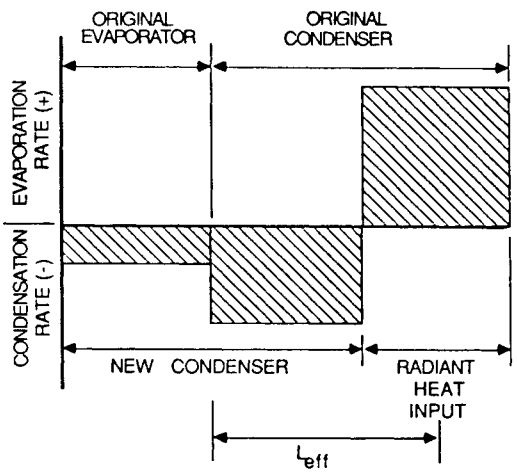

Fig. 11 Effective length for dryout prediction.

evaporator than in the uncovered portion of the condenser, the evaporator can still supply liquid return. Therefore, it is assumed that both parts act as a single condenser, as illustrated in Fig. 11. Since there is no adiabatic section, $L_{eff} = \frac{1}{2}(L_e + L_c) = L/2$. Although the percentages of the heat pipe used as an evaporator and as a condenser change with condenser coverage, the effective length remains the same.

When the heat pipe is on the verge of dryout, an energy balance for the radiant heat input zone yields

$$Q_{max} = A_s q_c - \sigma \epsilon A_s T^4 - C' \frac{dT}{dt} \qquad (10)$$

Equation (10) states that the maximum heat that can be transported out of the radiant heat input zone is equal to the radiant heat input minus the radiation heat loss and the thermal energy storage. The radiant heat flux necessary to reach the maximum transport rate can be calculated using Eqs. (4) and (10) and the relationship between C' and C [$C' = (A_s/A_{hp})C$]. Even though Eq. (9) is a steady-state equation, it can be used here because the liquid response to imposed pressure changes in the wick can be assumed to be instantaneous.[8,9] Table 5 shows the results of this calculation for the heat pipe initially operating at a steady-state temperature of 700°C at the onset of condenser heat input.

If a radiant heat flux exceeding the values given in Table 5 is applied, dryout may occur. Assuming the liquid response is instantaneous, the model can be used to predict liquid depletion rates and estimate the time to dryout.

Conclusions and Recommendations

The model developed provides a simple means of predicting the transient response of a liquid metal heat pipe. The model shows good agreement with the experimental data. It provides a means for predicting the internal vapor mass flow, evaporation, and condensation rates. This information is useful for predicting heat-pipe reversal and incipient failure.

Despite the wide variety of potential applications, there are a few limitations to the analytical model in its present form. Applications that involve condenser heat inputs near or in excess of the maximum capillary transport limit require a more complete modeling of liquid flow and storage in the wick. The model does not accurately predict local evaporator and condenser wall temperatures. To do this, the thermal resistances in the shell and wick would have to be included.

Acknowledgments

This research was cosponsored by the Air Force Office of Scientific Research and the Air Force Aero Propulsion Laboratory. The research was conducted at the Aero Propulsion Laboratory. Experiments were performed by Joe Gottschlich, Jill Johnson, and Don Reinmuller of AFWAL/POOA, and John Tennant of Universal Energy Systems Inc. Computer assistance was supplied by Steve Iden of AFWAL/POOA. The authors acknowledge the contributions and suggestions of Dr. Jerry Beam of AFWAL/POOA in the development of the analytical model reported here.

References

[1] Jacobson, D.L., "Sodium Heat Pipes and Thermal Energy Storage Systems," AFWAL-TR-81-2122, Jan. 1982.

[2] Olstad, S.J., Tanaka, F., and DeWitt, D.P., "Evaluation of a Method for Measuring Spectral Emissivity at Moderate Temperatures," AIAA Paper 85-0991, June 1985.

[3] Inconel Alloy 617, Huntington Alloys Inc., Huntington, WV.

[4] Vargaftik, N.B., *Tables on the Thermophysical Properties of Liquids and Gases*, 2nd ed., Hemisphere, 1975.

[5] Brennen, P.J. and Kroliczek, E.J., *Heat Pipe Design Handbook*, Vol. II, B and K Engineering, Towson, MD, June 1979.

[6] Tien, C.L. and Rohani, A.R., "Analysis of the Effects of Vapor Pressure Drop on Heat Pipe Performance," *International Journal of Heat and Mass Transfer*, Vol. 17, 1974, pp. 61–67.

[7] Chi, S.W., *Heat Pipe Theory and Practice*, McGraw-Hill, 1976, pp. 43, 55.

[8] Colwell, G.T. and Chang, W.S., "Measurement of the Transient Behavior of a Capillary Structure under Heavy Thermal Loading," *International Journal of Heat and Mass Transfer*, Vol. 27, No. 4, 1984, pp. 541–551.

[9] Beam, J.E., "Unsteady Heat Transfer in Heat Pipes," Ph.D. dissertation, School of Engineering, University of Dayton, OH, 1985.